Chapter 1

MIMO: Exploring the spatial dimension

1.1 Optical Spatial Modulation

1.1.1 Imaging SM and SMP System

A simple optical MIMO system using an ImR for VLC applications is illustrated in Figure **??**. Incoming data stream is coded and input to the modulator. The illumination state block provides a second input to the modulator which is the value of the average intensity to be emitted from each luminaire. Based on these inputs, the modulator block generates drive signals. N_{tx} number of lumianires positioned on the ceiling act as optical transmitters while providing illumination. LEDs in the luminaire convert modulated data in the electrical domain into optical signals in the visible spectrum (E/O and conversely O/E conversion). These optical signals propagate through the indoor space and are incident on the receiver. The receiver performs O/E conversion. With apriori knowledge of the implemented modulation and coding schemes, the electrical signal is then demodulated and decoded to recover the transmitted information. Figure **??** illustrates a schematic of an ImR. The optical assembly consists of a filter, imaging lens, aperture and housing. f is the focal length as set by the lens assembly. The sensor is made up of a matrix of N_{px} contiguous pixels. The length of the shortest side of each pixel is α_{px}^{min} and the pixel diagonal is α_{px}^{max}. The sensor is assumed to always be located distance f away from the optical

center of the lens.

The imaging optics acts as an optical demultiplexer. Based on the angle and the location of incidence, light rays are redirected by the imaging optics on to a specific path. This helps to decorrelate the channel matrix coefficients. Similarly, the ambient radiant flux incident at the aperture of the receiver is distributed among all pixels of the sensor. This helps to significantly reduce shot noise per pixel (**?**). The channel can then be modeled as

$$\mathbf{Y} = \mathbf{HX} + \mathbf{W} \tag{1.1}$$

where $\mathbf{X}$ is the intensity modulated input signal vector of length N_{tx}. The channel matrix $\mathbf{H}$ takes into account the path-loss, transmission of the optics and the respon-

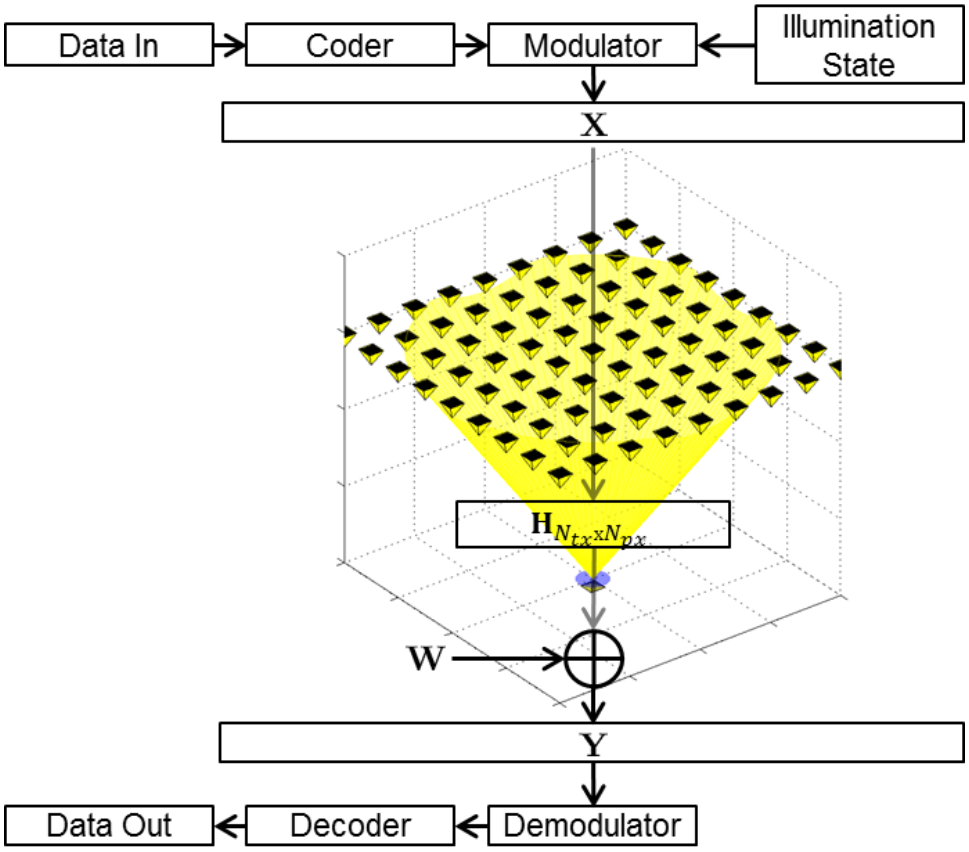

Figure 1·1: Schematic of an optical MIMO system.

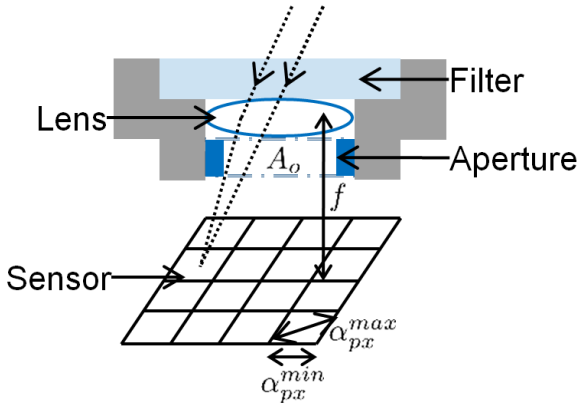

Figure 1·2: Schematic of an imaging receiver.

sivity of the sensor pixels. It can be computed as in reference (Butala et al., 2013). $\mathbf{Y}$ is the N_{px} length output current vector. $\mathbf{W} \sim \mathcal{N}(\mathbf{0}, \sigma^2 \mathbf{I}_{N_{px}})$ is the additive white Gaussian noise (AWGN) vector.

SM encodes $k = log_2(N_{tx})$ bits in the transmitter index in addition to $m = log_2(M)$ bits using M-ary modulation. Thus SM achieves spectral efficiency of $r = k + m = log_2(MN_{tx})$ bits/s/Hz. The incoming data stream is divided into r bits long symbols. First m bits of each symbol are mapped to one of the M-ary constellation points while the last k bits of each symbol select the luminaire that transmits the

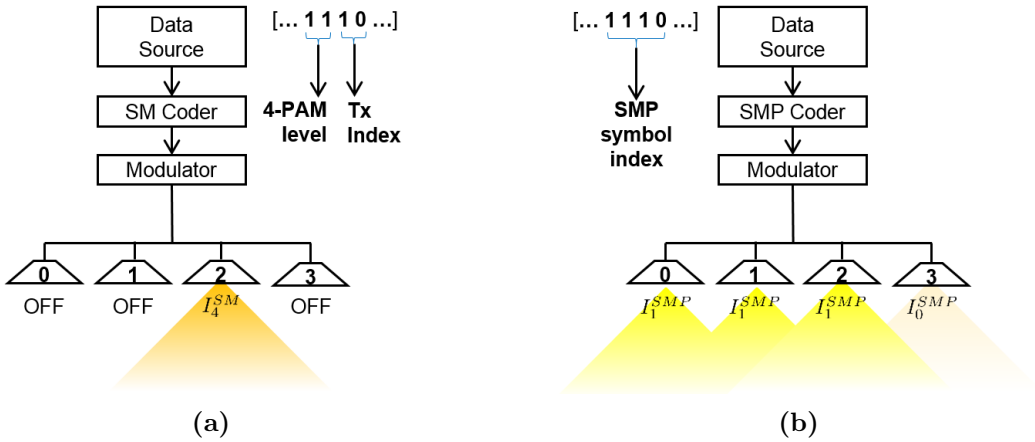

Figure 1·3: Illustration of (a) SM operation with $N_{tx} = 4$ and $M = 4$. (b) SMP operation with $N_{tx} = 4$ and $M = 2$.

selected constellation point. SM implementation is illustrated in Figure **??** for $N_{tx} = 4$ transmitters and 4-PAM (pulse amplitude modulation). M-PAM intensity levels for SM are selected as in (**??**) where I_{avg} is the average signal constraint to maintain desired illumination. Given a bit sequence forming a symbol [1 1 1 0], PAM level 3 (I_4^{SM}) is sent on transmitter index 2.

$$I_x^{SM} = \frac{2I_{avg}}{M+1}x; x = 1 \dots M \tag{1.2}$$

On the other hand, SMP uses all luminaires to jointly transmit information. If each of the N_{tx} luminaires can transmit M-ary modulation such that they jointly generate $M^{N_{tx}}$ unique symbols, spectral efficiency of SMP is given by $r = N_{tx}log_2(M)$ bits/s/Hz. Each r bit long section of the incoming data stream is then mapped to one of the $M^{N_{tx}}$ unique symbols. SMP for a setup with $N_{tx} = 4$ transmitters and 2-PAM is illustrated in Figure **??**. M-PAM intensity levels for SMP are selected as in (**??**) where I_{avg} is the average signal constraint to maintain desired illumination. A bit sequence forming a symbol [1 1 1 0] is jointly mapped to the 15^{th} out of $N_{tx}log_2(M) = 16$ possible unique symbols.

$$I_x^{SMP} = \frac{2I_{avg}}{M-1}x; x = 0 \dots M-1 \tag{1.3}$$

For a channel with equally likely symbols, a maximum likelihood detector is the optimal detector. If noise is AWGN, this reduces to nearest neighbor detection. Having observed $\mathbf{Y}$ and knowing $\mathbf{H}$, estimated symbol $\hat{\mathbf{X}}$ is the symbol closest to observation $\mathbf{Y}$ in Euclidean space. The signal detection can be written as

$$\begin{aligned} \hat{\mathbf{X}} &= \underset{\mathbf{X_i}}{\operatorname{argmax}}\, p_{\mathbf{Y}|\mathbf{X}}(\mathbf{Y}|\mathbf{X_i}, \mathbf{H}) \\ &= \underset{\mathbf{X_i}}{\operatorname{argmin}}\, ||\mathbf{Y} - \mathbf{H}\mathbf{X_i}||_F \end{aligned} \tag{1.4}$$

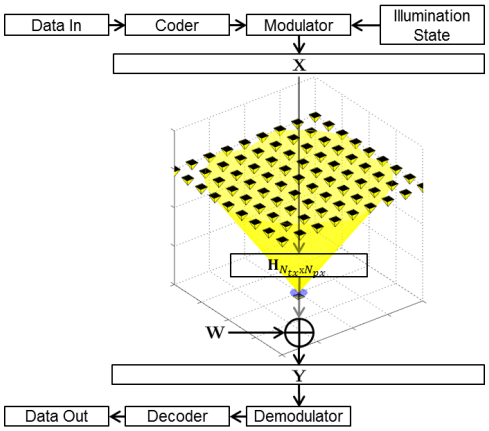

Figure 1·4: Optical MIMO System with Imaging Receiver

where $\mathbf{X_i}$ are the different symbols and $||.||_F$ is the Frobenius norm.

1.1.2 Imaging Spatial Modulation and Multiplexing

MIMO indoor optical systems implementing an imaging receiver have been shown to greatly increase the capacity of the channel over a SISO system operating under similar power constraints (Butala et al., 2013). Figure?? illustrates a simple optical MIMO system using an imaging receiver. Lumianires positioned on the ceiling act as optical transmitters while providing illumination. LEDs in the luminaire convert modulated data in the electrical domain into optical signals within the visible spectrum. These optical signals propagate through the indoor space and are captured by a sensor that performs optical to electrical conversion. The electrical signals are used to recover the data.

Imaging receivers for optical communication have been proposed in (?). The imaging optics act like an optical demultiplexer. Based on angle and location of incidence, light rays are redirected by imaging optics on to a specific path. This helps decorrelate channel matrix coefficients. This same phenomenon distributes the ambient radiant flux incident at the aperture of the receiver among all pixels of the sensor. This helps significantly reduce shot noise per pixel (?).

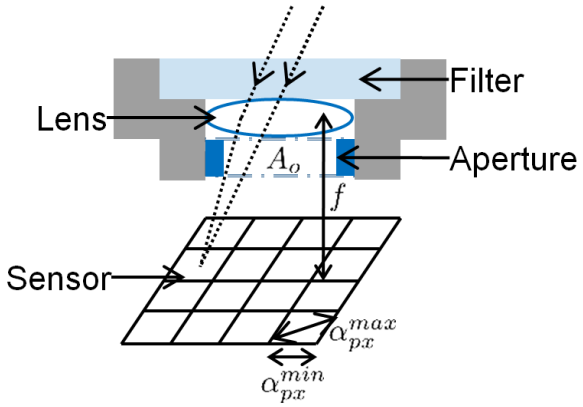

Figure 1·5: Schematic of Imaging Receiver

Figure?? illustrates a schematic of an imaging receiver. This is made up of an optical assembly and a sensor. The optical assembly consists of an optical filter, a lens assembly, an aperture and a housing to carry the parts. A_o is the area of the aperture opening. The lens assembly may consist of one or more lenses to minimize distortions. f is the focal length as set by the lens assembly. The sensor is made up of a matrix of contiguous pixels. The length of the shortest side of each pixel is α_{px}^{min}. It is assumed that there is some form of an on-chip bus architecture that routes the received signals to a receiving computer that performs the signal processing.

A MIMO indoor optical channel with imaging receiver can be modeled as (??). $\mathbf{X}$ is the intensity modulated input signal vector of length N_{tx}. $\mathbf{Y}$ is an N_{px} length vector containing output currents. $\mathbf{H}$ is the channel matrix taking into account the losses due to free space propagation, optical losses and channel decorrelation at the imaging optics and the responsivity of the receiver photodiodes. $\mathbf{W} \sim \mathcal{N}(\mathbf{0}, \sigma^2\mathbf{I_{px}})$ is the AWGN vector. Thermal noise is assumed the dominant source of noise (?). The N_{px}xN_{tx} channel matrix $\mathbf{H}$ is computed as in (Butala et al., 2013).

$$\mathbf{Y} = \mathbf{HX} + \mathbf{W} \tag{1.5}$$

For a channel with equally likely symbols, ML detector is the optimal detector. If

noise is AWGN, this reduces to NN detection. Having observed $\mathbf{Y}$ and knowing $\mathbf{H}$, estimated symbol $\hat{\mathbf{X}}$ is the symbol closest to observation $\mathbf{Y}$ in Euclidean space.

$$\begin{aligned}\hat{\mathbf{X}} &= \underset{\mathbf{X_i}}{\operatorname{argmax}}\, p_{\mathbf{Y}|\mathbf{X}}(\mathbf{Y}|\mathbf{X_i}, \mathbf{H}) \\ &= \underset{\mathbf{X_i}}{\operatorname{argmin}}\, ||\mathbf{Y} - \mathbf{H}\mathbf{X_i}||_F\end{aligned} \tag{1.6}$$

It is desired to analyze the effect of receiver configuration on performance of spatial multiplexing (SMux) and spatial modulation (SMod). An example system is considered which has 4 transmitters arranged on a regular grid with pitch P_{tx}. Each transmitter has side length α_{tx}^{min} and diagonal α_{tx}^{max}. The imaging receiver optics has focal length f. Sensor is made of large enough contiguous PD array such that all the 4 transmitter images (spots) fall on the sensor for all the different analysis configurations. Each PD is assumed to have a square shape with side length α_{px}^{min} and diagonal α_{px}^{max}. The receiver surface is assumed parallel to the transmitter plane. Receiver at a distance d from the transmitter plane sees a magnification $M = f/(d - f)$. If $d >> f$, which is true is most practical scenarios, $M \approx f/d$. The system performance is dependent on how the spots land on the PD array. Different system configurations can generate similar spot profile on the sensor and thus similar BER performance. To analyze the system performance independent of a specific system configuration, the following normalization parameters are defined.

Normalized Luminaire Side Length

The normalized luminaire side length α_s is defined as the ratio of the diagonal of a spot to side length of a PD.

$$\alpha_s \equiv \frac{Ma_{tx}^{max}}{\alpha_{px}^{min}} \tag{1.7}$$

α_s specifies the spot size relative to the sensor dimensions. For example, consider two similar systems which differ in only the luminaire diagonal and PD side lengths. If both parameters differ in scale by the same factor, α_s would remain the same for both systems. $\alpha_s \leq 1$ implies the spot size is at most as large as the size of a PD. If the centroid of the spot is aligned with the centroid of a PD, the spot will lie completely inside the PD.

Normalized Luminaire Pitch

The normalized luminaire pitch δ_s is defined as the ratio of the spot pitch to the length PD diagonal.

$$\delta_s \equiv \frac{MP_{tx}}{\alpha_{px}^{max}} \tag{1.8}$$

δ_s specifies the distance between the centroids of adjacent spots relative to the sensor dimensions. For example, now consider two similar systems which differ in only the transmitter pitch and PD diagonal. If both parameters differ in scale by the same factor, δ_s would remain the same. $\delta_s > 1$ ensures that centroids of adjacent spots lie on different pixels. In the limit, if both transmitters were point sources, condition $\delta_s > 1$ would ensure that different pixels receive signals from neighboring transmitters, thus eliminating ICI.

Normalized Luminaire Edge-Edge Distance

The normalized luminaire edge-edge distance η_s is defined as the ratio of minimum distance between the edges of adjacent spots to the length of the pixel diagonal.

$$\eta_s \equiv \frac{M(P_{tx} - \alpha_{tx}^{max})}{\alpha_{px}^{max}} \tag{1.9}$$

η_s specifies the minimum possible distance between the edges of adjacent spots relative to the sensor dimensions. For example, now consider two similar systems which differ in only the minimum possible distance between the edges of adjacent luminaires and PD diagonal. If both parameters scaled by the same factor, η_s would remain the same. $\eta_s > 1$ ensures that adjacent spots do not overlap on any pixel. η_s can be expressed in terms of α_s and δ_s as in (**??**). For square pixels, $l = 1/\sqrt{2}$.

$$l = \frac{\alpha_{px}^{min}}{\alpha_{px}^{max}} \tag{1.10}$$

$$\eta_s = \delta_s - l\alpha_s \tag{1.11}$$

Normalized Magnification

Let M_0 be the magnification of the system when $\alpha_s = 1$. Normalized magnification is defined as the ratio of the magnification of the system to M_0.

$$M_0 \equiv \frac{\alpha_{rx}^{min}}{\alpha_{tx}^{max}} \tag{1.12}$$

$$\mu_s \equiv \frac{M}{M_0} \tag{1.13}$$

Consider two similar systems that differ in distance between the luminaire plane and the receiver and also in the receiver focal lengths. μ_s for both systems is the same value when both parameters differ in scale by the same factor.

In an indoor VLC system, luminaires need to maintain an average emitted radiant flux over different overlapping time windows so that the perceived illumination remains constant. Thus a fair performance comparison between different modulation schemes can be made when they emit the same radiant flux. Thus the SNR is defined

as

$$SNR = \frac{(hP_{avg}^{tx})^2}{\sigma^2} \tag{1.14}$$

where P_{avg}^{tx} is the average radiant flux emitted by a transmitter, h is the optical to electrical conversion factor ($AW^{-1}\Omega^{-2}$) and σ^2 is the noise power. Without loss of generality, $h = 1$ is assumed. This is similar definition as in (Fath and Haas, 2013)

1.1.3 Results

The effects of varying transmitter array and ImR configurations on the BER performance of SM and SMP systems are studied using simulations. An array of 4 transmitters that are arranged on a regular grid with pitch P_{tx} is considered. Using PAM, and to achieve 4 bits/sym, SM with $N_t = 4$ and $M = 4$ and SMP with $N_t = 4$ and $M = 2$ are implemented. To achieve 8 bits/sym, SM with $N_t = 4$ and $M = 64$ and SMP with $N_t = 4$ and $M = 4$ are implemented. The distance d between the transmitter and receiver planes is $2m$. Lambertian luminaires of order $m = 1$ are assumed to have a spectral power distribution that is approximated by a sum of gaussians as in (**?**). The responsivity of each pixel is equal to $0.4A/W$. Within this context, it is assumed that the pixels array is large enough to ensure that each of the four spots fall on the sensor for each of the different configurations considered below.

Using the parameters specified above, the channel gains are of the order of 10^{-7} for all simulations. Thus the transmitted signal power is about 140dB higher than the received signal power. Typically, the SNR is defined as the ratio of received signal power to noise power. However, given SNR as defined in (XYZ), there is an offset of at least +140dB over typical definition.

Imaging vs Non-Imaging Receiver

Performance gains of using an ImR over a NImR are analyzed in this subsection. The transmitter and modulation parameters are the same as described above. For this analysis, $P_{tx} = 0.5m$ is considered. The NImR is made up of 2×2 array of pixels; each with a side length of 1 mm and a pitch of 1 mm. Each pixel has a concentrator of refractive index 1.5 and field-of-view (FOV) of 60 deg. For the ImR, the sensor is modeled as 2×2 array of pixels with side length and pitch of $1mm$. The imaging lens is defined to have sufficient magnification to align the images of the four transmitters each with four pixels respectively. The FOV of the receiver changes with the sensor dimensions. The maximum FOV is defined as 60 deg; the same as in NImR case. A fair performance comparison between the two receiver configurations can be made under the assumption that the same signal radiant-flux is incident on both. Thus, the aperture of the ImR is modeled to have an area of $1mm^2$.

BER vs SNR curves for SM and SMP using NImR and ImR are shown in Figure **??**. At low signal powers, using a NImR, shot noise is the dominant source of noise. At high signal powers, inter-channel-interference (ICI) dominates the noise for an NImR because the channel matrix coefficients are highly correlated. This can be seen as two regions of the BER curves when using a NImR. SM mitigates ICI and is thus more robust as compared to SMP in this scenario. BER achieved by SMP with NImR are greater than 10^{-3} for the range of SNR considered and thus cannot be improved by forward error correction (FEC). SM needs a high transmit signal power to achieve BER= 10^{-3} for both 4 and 8 bits/sym. Conversely, ImR completely demultiplexes the four transmit signals while generating a diagonal channel matrix and thus avoids ICI under ideal setup. To achieve BER= 10^{-3} at 4 bits/sym, SM with ImR performs about 8dB better that SMP with ImR and about 45dB better than SM with NImR. SMP packs more bits spatially in transmitter location as compared to SM. Thus, to

achieve higher spectral efficiency while keeping the number of transmitters the same,

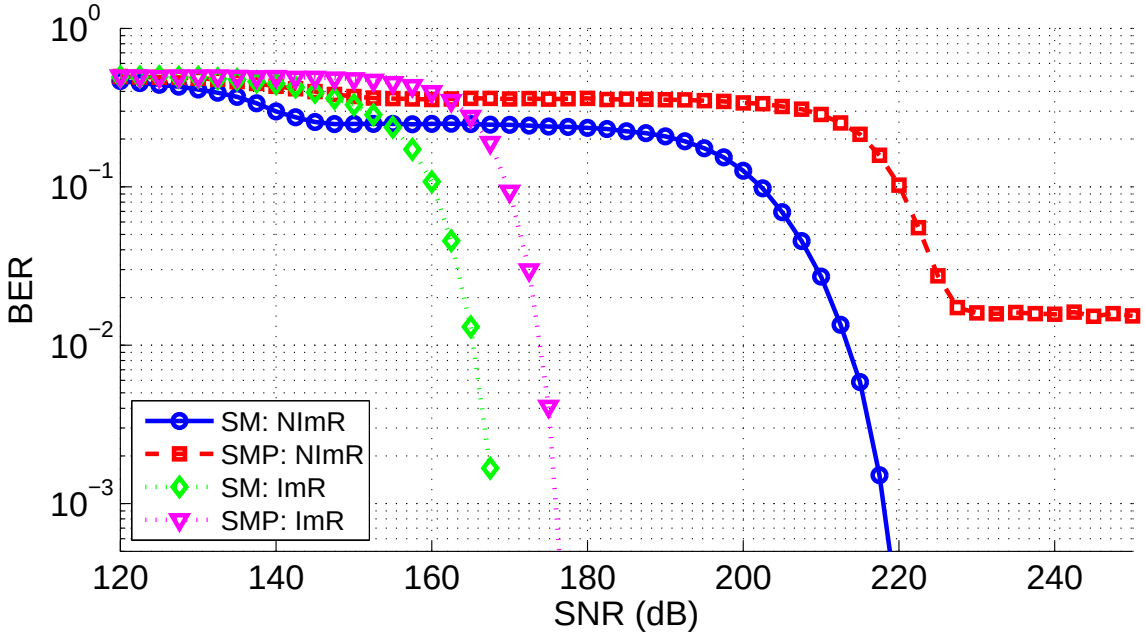

(a) 4 bits/sym

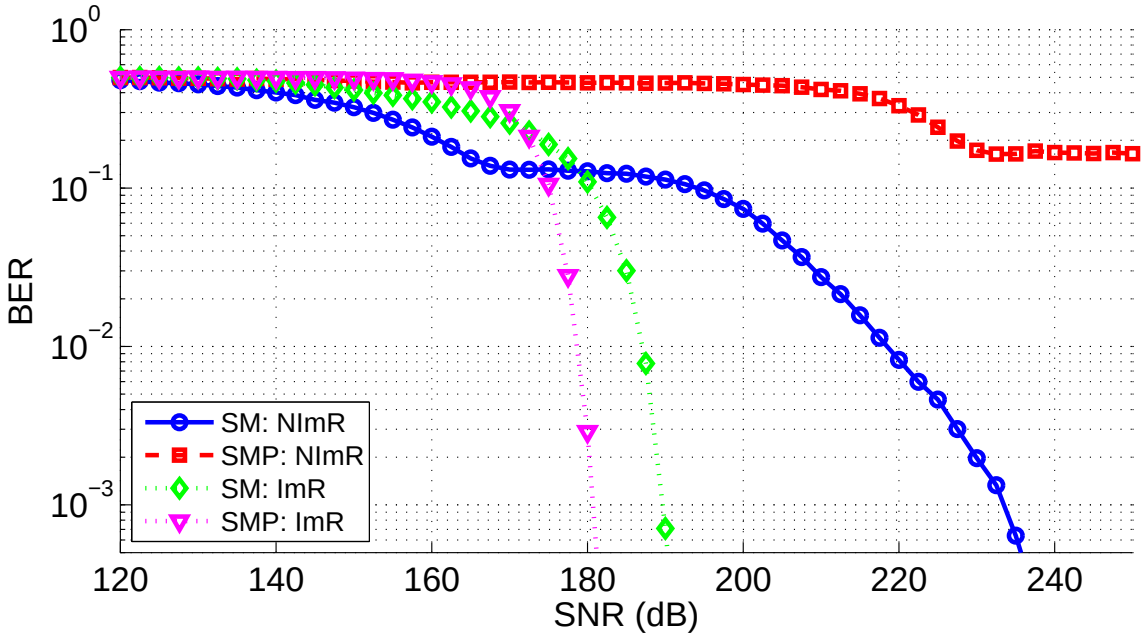

(b) 8 bits/sym

Figure 1·6: Performance comparison of SM and SMP using non–imaging an imaging receiver.

more PAM levels are needed for SM as compared to SMP thus quickly degrading SM's performance. To achieve BER= 10^{-3} at 8 bits/sym, SMP with ImR outperforms SM with ImR by about 10dB and SM with NImR by about 52dB. The channel matrix coefficient decorrelation afforded by ImR provide huge SNR gains over NImR for a given BER.

Varying α_s

For this analysis, α_s is varied while keeping δ_s and μ_s fixed. As illustrated in Figure **??**, α_s affects only the spot size. As α_s increases, spots on the sensor overlap increasingly more number of pixels degrading the BER performance. Increasing the number or pixels per spot also increases the noise for each link thus causing the drop in performance. Very small pixel sizes or very large transmitter sizes also cause increase in α_s. A smaller pixel size does enable the system to pack more channels provided α_s is relatively small. On the other hand, having very small pixel sizes or alternately large transmitter illumination surface tend to increase α_s and force the system to operate in a suboptimal configuration.

BER vs SNR curves for SM and SMP for different values of α_s are shown in Figure **??**. To achieve BER$\leq 10^{-3}$ at 4 bits/sym, SNRs of about [168,168,170,173]dB and [176,176,178,181]dB are needed for α_s=[0.5,1,1.41,2] with SM and SMP respectively. To achieve BER$\leq 10^{-3}$ at 8 bits/sym, SNRs of about [190,190,192,195]dB and [181,181,183,186]dB are needed for α_s=[0.5,1,1.41,2] with SM and SMP respectively. Thus there is about a 2dB SNR penalty for system operating at $\alpha_s = 1.41$ and 5dB SNR penalty for system operating at $\alpha_s = 2$ as compared to that at $\alpha_s = 1$.

Varying η_s

For this analysis, η_s (alternately δ_s) is varied while keeping α_s and μ_s fixed. Thus only the effect of change in spot pitch affects the BER performance. As illustrated in Figure **??**, as η_s increases, distance between the spots on the sensor increases as they push further apart.

BER vs SNR curves for SM and SMP for different values of η_s are shown in Figure **??**. To achieve BER$\leq 10^{-3}$ at 4 bits/sym, SNRs of about [167,174,172,170]dB and [175,182,180,178]dB are needed for η_s=[0,0.71,1,1.41] with SM and SMP respectively. To achieve BER$\leq 10^{-3}$ at 8 bits/sym, SNRs of about [189,196,194,192]dB and [180,187,185,183]dB are needed for η_s=[0,0.71,1,1.41] with SM and SMP respectively. We see that the BER performance is best when the spot overlaps minimum number of pixels and worst when the spot is centered at a corner of a pixel thus maximizing

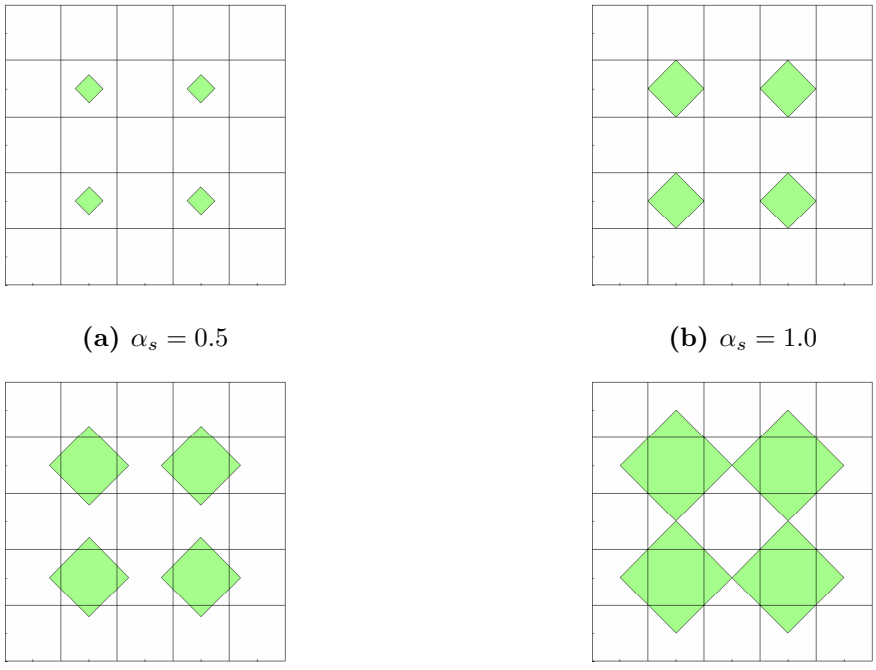

(a) $\alpha_s = 0.5$ **(b)** $\alpha_s = 1.0$

(c) $\alpha_s = 1.41$ **(d)** $\alpha_s = 2.0$

Figure 1·7: Spots on the sensor for different α_s

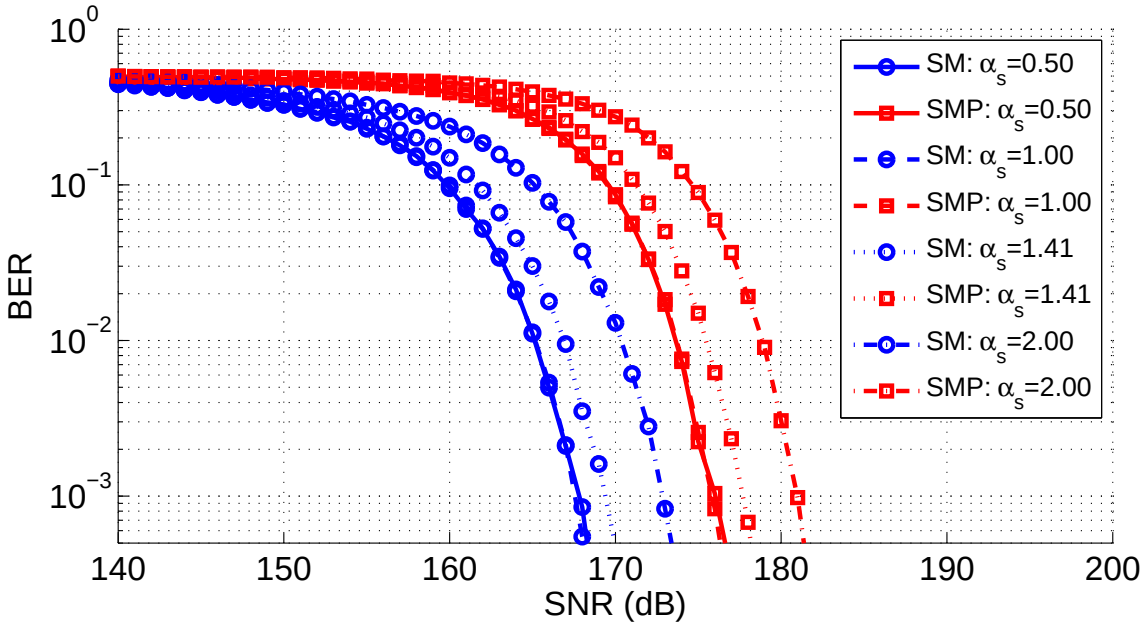

(a) 4 bits/sym

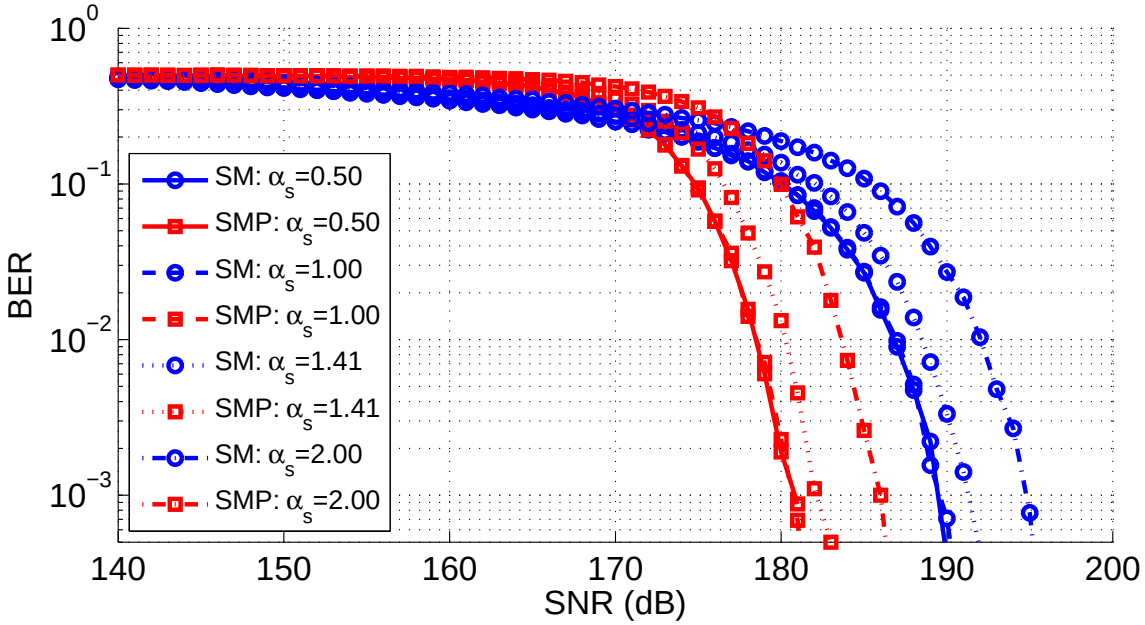

(b) 8 bits/sym

Figure 1·8: BER vs SNR for different α_s.

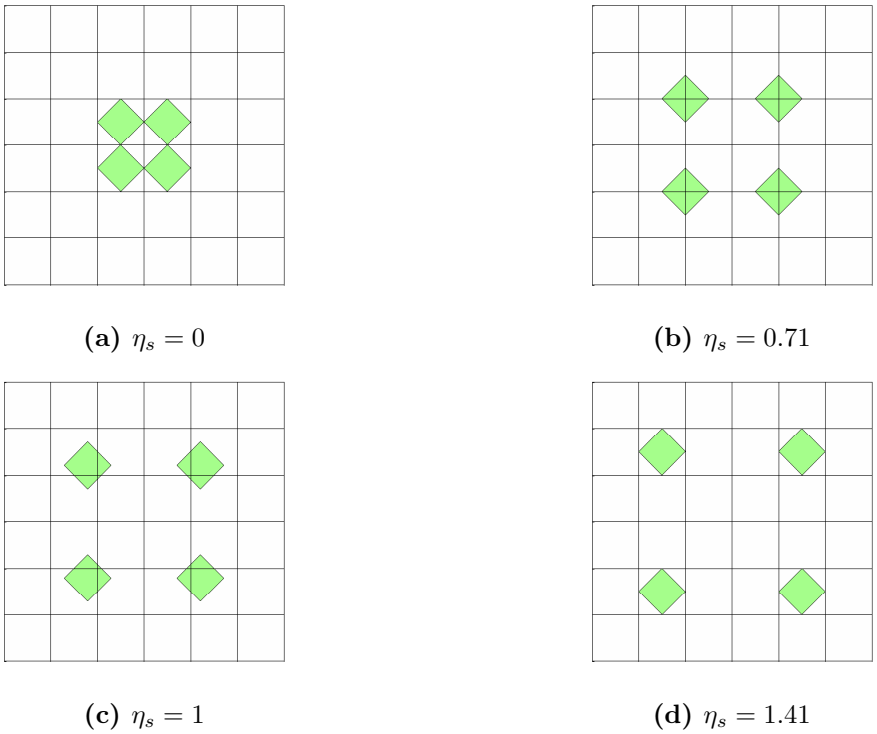

(a) $\eta_s = 0$ **(b)** $\eta_s = 0.71$

(c) $\eta_s = 1$ **(d)** $\eta_s = 1.41$

Figure 1·9: Spots on sensor for different η_s

the number of pixels it overlaps with. In this setup, for BER= 10^{-3}, there is an SNR penalty of about 7dB between the best and worst cases. The slight drop in performance for $\eta_s = 1.4$ as compared to $\eta_s = 0$ can be attributed to drop in free-space gain caused by the larger distance per link longer as a result of increased transmitter pitch.

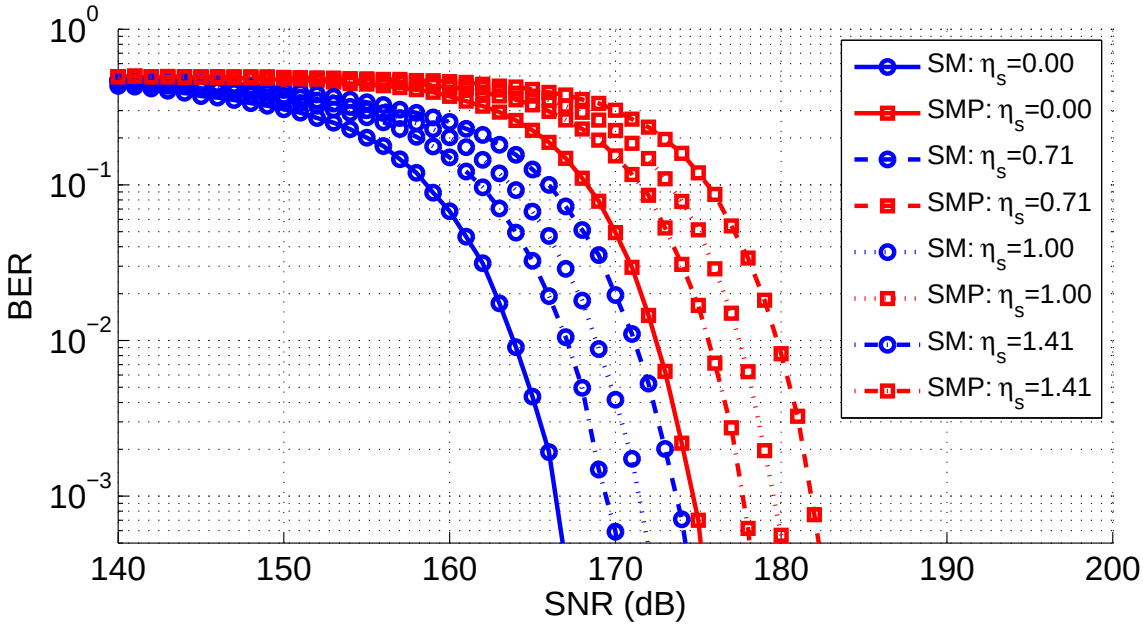

(a) 4 bits/sym

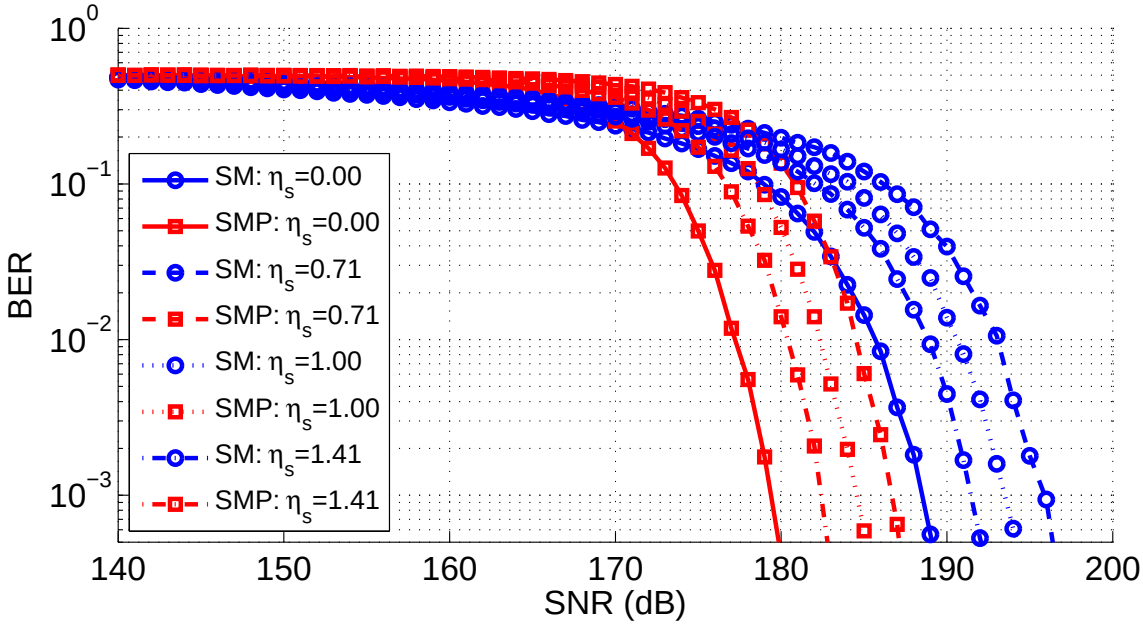

(b) 8 bits/sym

Figure 1·10: BER vs SNR for different η_s.

Varying μ_s

In this analysis, μ_s is varied by varying f. Alternately, it can be varied by changing d. Varying μ_s affects both α_s and η_s simultaneously. This captures their combined impact on the BER performance. We see from Figure **??** that increasing μ_s not only increases the spot size but also pushes the spots away from each other. Note unlike in previous case, the transmitter pitch remains constant ($P_{tx} > 0$).

BER vs SNR curves for SM and SMP for different values of μ_s are shown in Figure **??**. To achieve BER= 10^{-3} at 4 bits/sym, SNRs of about [167,173,169,173]dB and [175,181,177,181]dB are needed for μ_s=[0.5,1,1.41,2] with SM and SMP respectively. To achieve BER= 10^{-3} at 8 bits/sym, SNRs of about [189,195,191,195]dB and [180,186,182,186]dB are needed for μ_s=[0.5,1,1.41,2] with SM and SMP respectively.

The best performance is obtained for $\mu_s \leq 0.5$. This is because at this value of μ_s, $\alpha_s < 1$ and η_s is such that all spots lie on different adjacent pixels. It can also be inferred that given enough transmitters in the room, at $\mu = 0.5$, every single pixel could get signal from a single transmitter thus greatly improving the capacity of the channel. If the luminaires transmit with different power levels or if the channels gains are significantly different, capacity maximizing μ_s is an optimization problem to be solved in the future.

At lower bit rates, SM benefits from having higher transmit power per symbol at lower M-PAM level. To achieve higher bit-rates, higher M-PAM levels push the constellations closer to each other thus quickly degrading the SM performance as compared to SMP. As shown in Figure **??**, Figure **??** and Figure **??**, to achieve BER= 10^{-3}, at 4 bits/sym, SM performs 8-10dB better while at 8 bits/sym, SMP performs 8-10dB better.

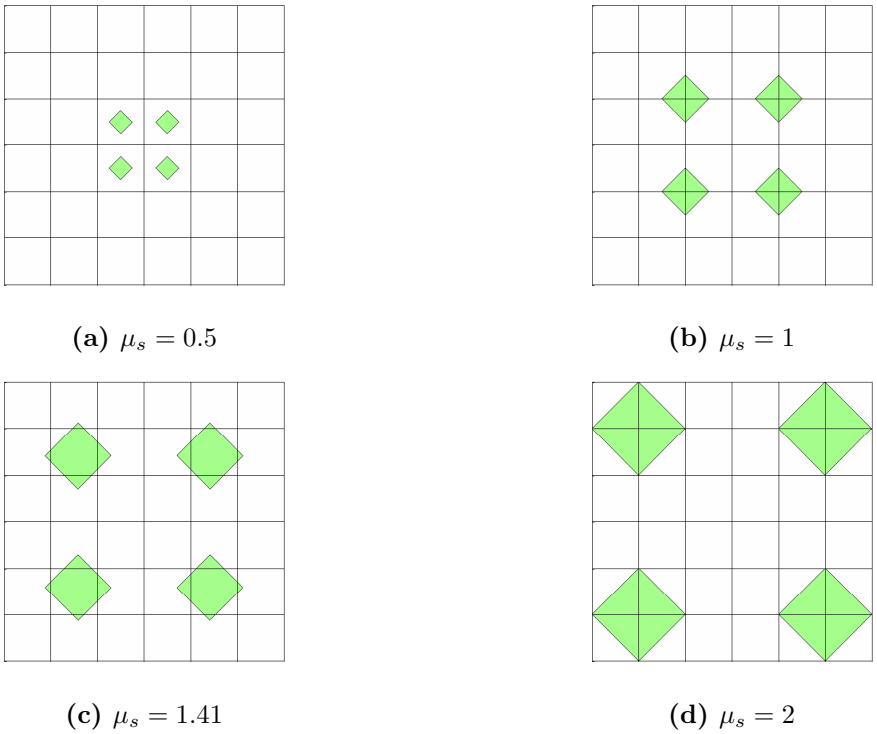

(a) $\mu_s = 0.5$ **(b)** $\mu_s = 1$

(c) $\mu_s = 1.41$ **(d)** $\mu_s = 2$

Figure 1·11: Spots on sensor for different μ_s.

1.2 Sample Indexed Spatial Orthogonal Frequency Division Multiplexing

Recently, the increase in use of portable computing devices has created an intense demand for wireless data access. Spectral allocations and regulations limit our ability to increase the capacity of existing channels within the radio frequency (RF) spectrum. Advances made in the solid-state lighting industry are driving significant deployments of energy-efficient light emitting diode (LED) based luminaries. This has created an opportunity to use such luminaries to establish high capacity indoor visible light communication (VLC) links and reduce the bottleneck on existing RF wireless channels. Under this model, luminaries simultaneously support illumination and wireless data transmission (Elgala et al., 2011). OSM and O-OFDM are two techniques that have been proposed to implement such a dual-use VLC channel.

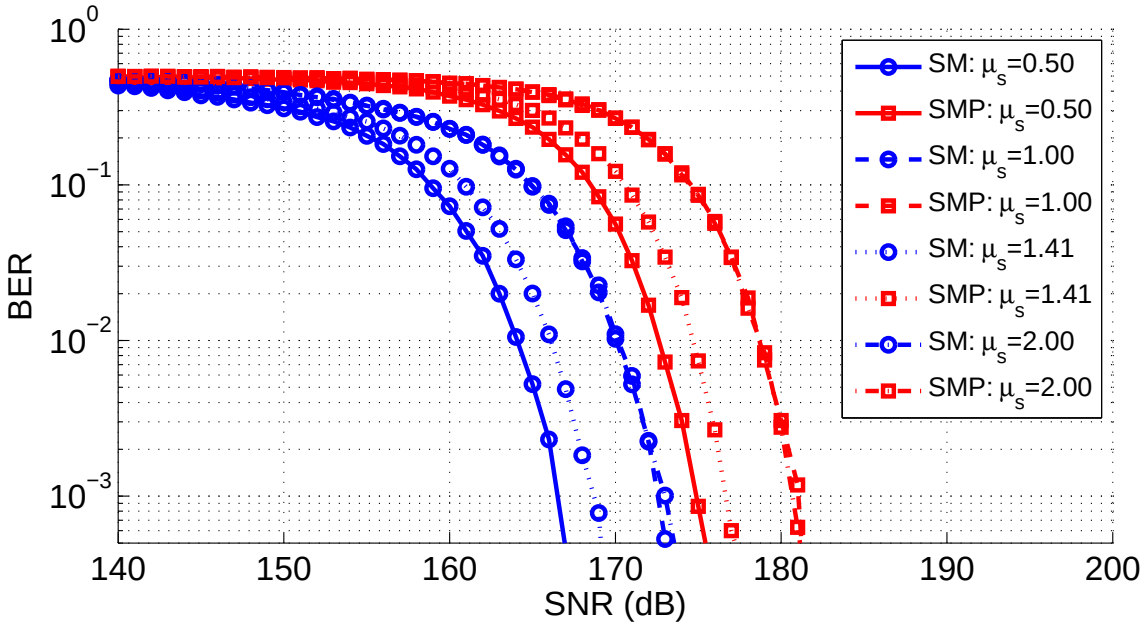

(a) 4 bits/sym

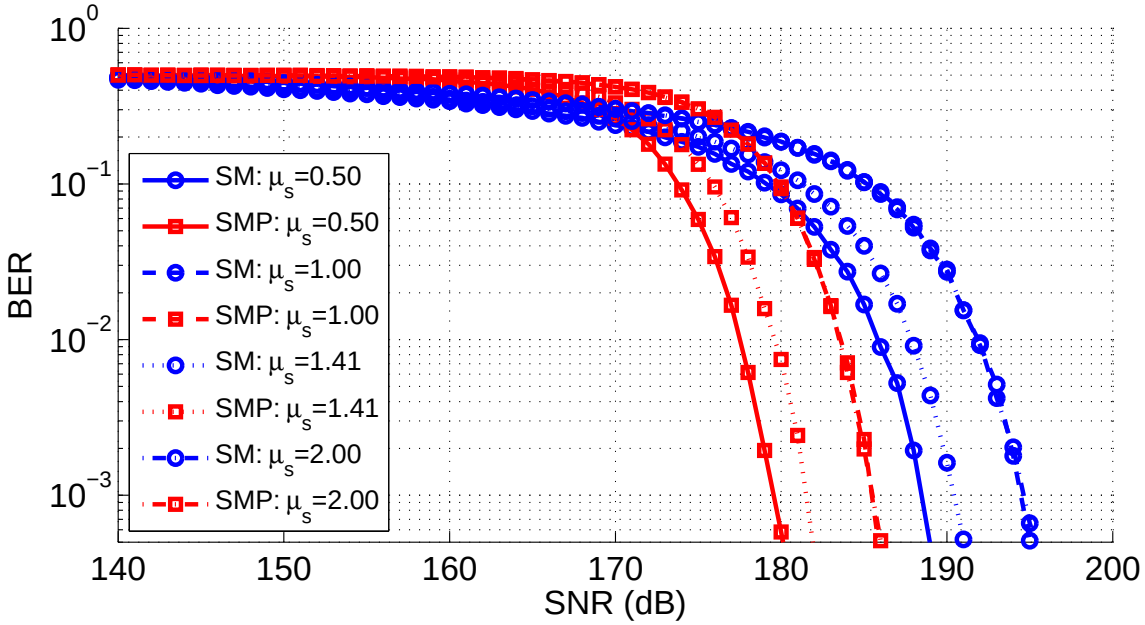

(b) 8 bits/sym

Figure 1·12: BER vs SNR for different μ_s.

OSM is a multiple-transmitter technique in which information is encoded over (a) index of luminiares that are spatially separated and (b) modulation scheme overlayed on indexed luminaire (Mesleh et al., 2010). Within a symbol period, only one luminaire emits a radiant flux while all other luminaires are idle. This minimizes the inter-channel interference (ICI) thus simplifying the detection process and the overall system complexity as compared to spatial multiplexing (SMP). In OSM, the bit-stream to be transmitted is divided into contiguous sections of $k = log_2(N_{tx})$ spatial bit-stream and $m = log_2(M)$ modulation bit-stream where N_{tx} is the number of luminaires and M is the modulation order. The k bits select the luminaire to be activated while the m bits select the M-ary modulation symbol to be transmitted. Thus, OSM system provides $log_2(MN_{tx})$ bits per symbol. In (Fath et al., 2011), an OSM system with pulse amplitude modulation (PAM) as the overlayed modulation scheme is proposed. Reference (Popoola et al., 2012) proposes a scheme that combines OSM with pulse position modulation (PPM) to benefit from the energy efficiency of PPM as compared to PAM. Reference (Butala et al., 2014) shows ImR can provide significant SNR gains for OSM and SMP as compared to NImR.

Implementation and performance comparisons of ACO-OFDM and DCO-OFDM is shown in reference (Mesleh et al., 2011). In ACO-OFDM, data is assigned only on odd subcarriers while in DCO-OFDM all odd and even subcarriers are assigned data. Hermetian symmetry is enforced across the frequency-domain O-OFDM symbol. An inverse fast fourier transform (IFFT) process then results in a real-valued time domain signal that multiplexes the streams before transmission over the channel. In IM/DD systems, the signal is transmitted by varying the output flux from the transmitter. Thus, the transmitted signal must be non-negative and real valued. The ACO-OFDM signal can be clipped at values below zero because the resulting clipping noise is shown to be orthogonal to the signal (Armstrong and Lowery, 2006). Conversely, in DCO-

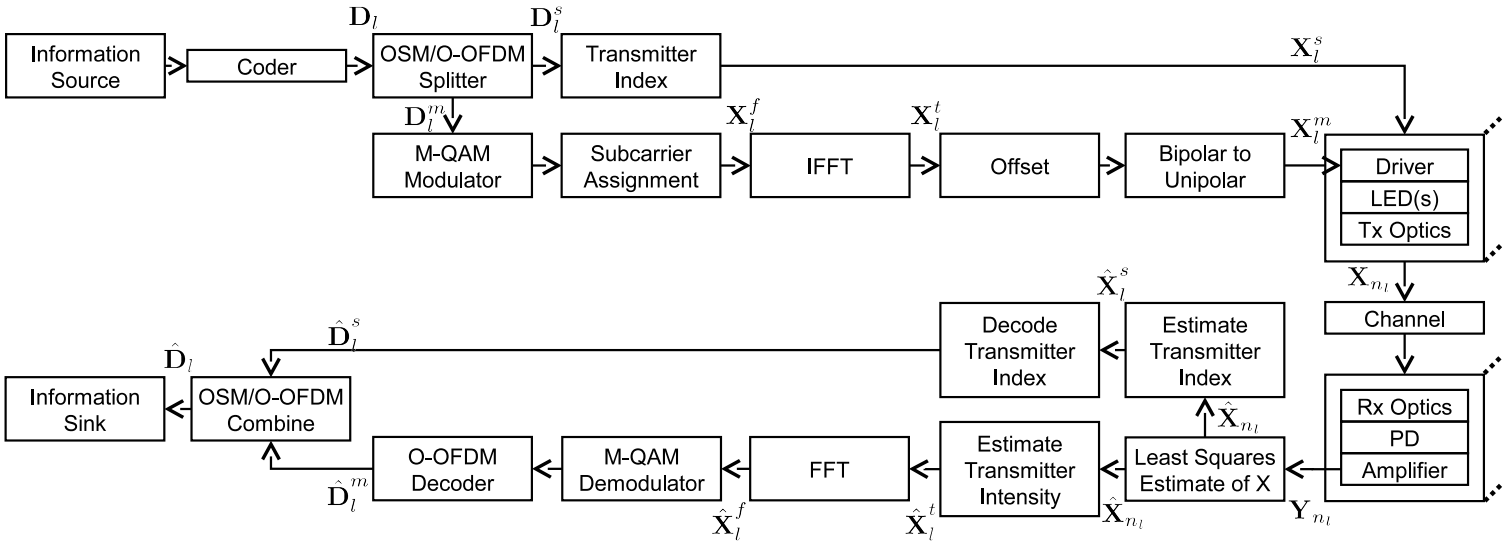

Figure 1·13: Block diagram of system implementing SIS-OFDM

OFDM an offset must be added to the multiplexed signal in order to minimize errors due to clipping of negative valued signal. O-OFDM achieves high spectral efficiency by enabling parallel transmission of higher order modulation symbols on orthogonal subcarriers. The number of data-subcarriers, N_{sc}^{d}, equals $(N_{sc}/4)$ for ACO-OFDM and $(N_{sc}/2-1)$ for DCO-OFDM where N_{sc} is the total number of subcarriers. Thus the number of transmitted bits per O-OFDM symbol is given by $R^{m} = N_{sc}^{d} \times log_2(M)$.

An approach to combine OSM and traditional OFDM is proposed in reference (Ganesan et al., 2006). This approach is adapted for IM/DD communications in reference (Zhang et al., 2012). Here, an incoming bit-stream is divided into O-OFDM and OSM streams. Data from O-OFDM stream is assigned to different subcarriers to form the frequency domain O-OFDM symbol. OSM is then implemented in the frequency domain where each data-subcarrier is assigned to a transmitter determined by the spatial bit-stream. An IFFT operation is implemented at each transmitter to multiplex the data before transmission. Spectral efficiency of this scheme is then proportional to the number of data-subcarriers. In comparison, the spectral efficiency of SIS-OFDM is proportional to the number of subcarriers which is equal to at least double the number of data-subcarriers. Additionally, the SIS-OFDM system requires a single IFFT operation, independent of the number of transmitters and thus maintains a computational complexity equal to that of SISO OFDM transmission. Finally, SIS-OFDM using an ImR achieves much better power efficiency as compared to equivalent system using NImR.

Figure3·1 illustrates the block diagram of a system implementing SIS-OFDM. The information source generates the input data-stream. The coder converts the data-stream into a binary bit-stream $\mathbf{D}$ which is divided into consecutive segments of $R^{ms} = R^{m} + R^{s}$ bits where $R^{s} = N_{sc} \times k = N_{sc} \times log_2(N_{tx})$ is the number of spatial bits . Let the l^{th} such segment be denoted by $\mathbf{D}_l$. The first R^{m} bits of $\mathbf{D}_l$ are

collected in a vector $\mathbf{D}_l^m$ are are mapped by an M-QAM modulator. The generated QAM symbols are then assigned to subcarriers (based on the O-OFDM signal format, *i.e.* DCO-OFDM or ACO-OFDM) to generate a frequency-domain O-OFDM symbol $\mathbf{X}_l^f$ of length N_{sc}. An IFFT operation is applied on $\mathbf{X}_l^f$ to produce a real-valued bipolar time-domain O-OFDM symbol $\mathbf{X}_l^t$ of the same length N_{sc}. The latter R^s bits of $\mathbf{D}_l$ are collected in a vector D_l^s and are mapped to N_{sc} length transmitter index vector denoted by $\mathbf{X}_l^s$. Let $\mathbf{X}_l^m$ denote the real unipolar baseband signal after biasing and/or clipping, and $0 \leq n_l \leq (N_{sc} - 1)$ indicate the relative time index for the next SIS-OFDM symbol to be transmitted. At each time instance, an O-OFDM signal value from $\mathbf{X}_l^m$ is transmitted from a luminaire indexed by $\mathbf{X}_l^s$. Let $\mathbf{X}_{n_l}$ be this N_{tx} length transmission vector at time instant n_l. Thus the j^{th} element of this vector is then given by

$$\mathbf{X}_{n_l}(j) = \begin{cases} \mathbf{X}_l^m(n_l) & ; j = \mathbf{X}_l^s(n_l) \\ 0 & ; \text{else} \end{cases} \tag{1.15}$$

The SIS-OFDM symbol and transmit vector generation is explained using the following example which considers ACO-OFDM with $N_{sc} = 8$, 4-QAM subcarrier modulation and $N_{tx} = 2$. Here, $R^m = 4$ and $R^s = 8$, *i.e* $R^{ms} = 4 + 8 = 12$ bits per SIS-OFDM symbol. The assumed bits forming one SIS-OFDM symbol $\mathbf{D}_l$ are shown in Table 3.1. Table 3.2 then illustrates the data to subcarrier and transmitter index assignments. In this example, the transmitters would jointly transmit vector $\mathbf{X}_{n_l} = [0\ \sqrt{2}]^T$ at relative time index $n_l = 2$.

Stream	**Bits**
$\mathbf{D}_l$	$[\ 1\ 1\ 0\ 0\ 0\ 1\ 1\ 0\ 0\ 0\ 1\ 1\ ]^T$
$\mathbf{D}_l^m$	$[\ 1\ 1\ 0\ 0\ ]^T$
$\mathbf{D}_l^s$	$[\ 0\ 1\ 1\ 0\ 0\ 0\ 1\ 1\ ]^T$

Table 1.1: Example SIS-OFDM data streams using ACO-OFDM

n_l	**OFDM bits**	$\mathbf{X}_l^f$	$\mathbf{X}_l^t$	$\mathbf{X}_l^m$	**SM bits**	$\mathbf{X}_l^s$
0	-	0	0	0	0	1
1	1 1	$-1-j$	-1	0	1	2
2	-	0	$\sqrt{2}$	$\sqrt{2}$	1	2
3	0 0	$1+j$	1	1	0	1
4	-	0	0	0	0	1
5	-	$1-j$	1	1	0	1
6	-	0	$-\sqrt{2}$	0	1	2
7	-	$-1+j$	-1	0	1	2

Table 1.2: Example subcarrier and luminaire assignment

The indoor optical MIMO channel is modeled as,

$$\mathbf{Y}_{n_l} = \mathbf{H}\mathbf{X}_{n_l} + \mathbf{W}_{n_l} \tag{1.16}$$

where $\mathbf{X}_{n_l}$ is the instantaneous transmit vector. $\mathbf{H}$ is the channel matrix and can be computed as in (Butala et al., 2013). $\mathbf{Y}_{n_l}$ is the received signal vector and $\mathbf{W}_{n_l}$ is zero-mean additive white gaussian noise (AWGN) vector.

The receiver can be configured such that $\mathbf{H}$ is of rank N_{tx}. In that case, $(\mathbf{H}^*\mathbf{H})^{-1}$ exists. The least squares estimate of transmitted vector $\mathbf{X}_{n_l}$ can be computed as

$$\hat{\mathbf{X}}_{n_l} = (\mathbf{H}^*\mathbf{H})^{-1}\mathbf{H}^*\mathbf{Y}_{n_l} \tag{1.17}$$

In SIS-OFDM, only one luminaire emits radiant flux at a given time instance. Thus the maximum element of $\hat{\mathbf{X}}_{n_l}$ is estimated as the transmitted signal flux $\hat{x}_{n_l}^m$.

$$\hat{x}_{n_l}^m = \max_{\forall j}(x_j)\,; x_j \in \hat{\mathbf{X}}_{n_l} \tag{1.18}$$

The index of $\hat{x}_{n_l}^m$ within $\hat{\mathbf{X}}_{n_l}$ provides an estimate of the active luminaire. Thus the instantaneous luminaire index $\hat{x}_{n_l}^s$ is estimated as

$$\hat{x}_{n_l}^s = \operatorname*{idxmax}_{\forall j}(x_j)\,; x_j \in \hat{\mathbf{X}}_{n_l} \tag{1.19}$$

A SIS-OFDM symbol is transmitted over N_{sc} time slots. $\hat{x}^m_{n_l}$ and $\hat{x}^s_{n_l}$ are estimated for each time slot n_l and collected in vectors $\hat{\mathbf{X}}^m_l$ and $\hat{\mathbf{X}}^s_l$ respectively. $\hat{\mathbf{X}}^m_l$ is subject to signal processing to recover the transmitted O-OFDM signal in $\hat{\mathbf{X}}^t_l$. An FFT process then demultiplexes the data and estimates the transmitted O-OFDM symbol in $\hat{\mathbf{X}}^f_l$. Maximum likelihood (ML) estimation is performed on the received symbols over the N^d_{sc} data-subcarriers to estimate the bits transmitted and collected in $\hat{\mathbf{D}}^m_l$. The transmitter indexes estimated in $\hat{\mathbf{X}}^s_l$ are subject to decimal to k-length binary conversion to decode the spatial bits as $\hat{\mathbf{D}}^s_l$. The estimated OSM and O-OFDM bits are then combined to estimate the transmitted l_{th} bit-stream as $\hat{\mathbf{D}}_l$.

The SIS-OFDM scheme explained above can provide up to R^s additional bits per symbol over equivalent SISO O-OFDM transmission. The system explored in (Zhang et al., 2012) can transmit $(N^d_{sc} \times k)$ spatial-bits per symbol as compared to $(N_{sc} \times k)$ spatial-bits per symbol in SIS-OFDM. Thus using SIS-OFDM provides additional spectral efficiency gain of $(3 \times N_{sc} \times k/4)$ bits per symbol while using ACO-OFDM and $((N_{sc}/2 - 1) \times k)$ bits per symbol while using DCO-OFDM.

Two comparable 4×4 MIMO systems, using ImR and NImR respectively, implementing SIS-OFDM with ACO-OFDM and DCO-OFDM are simulated to evaluate the system performance. The $N_{tx} = 4$ lambertian transmitters of order 1 are assumed located on the ceiling of a room, facing vertically down, and at $0.5m$ pitch. The transmitters are assumed to have a linear electrical to optical conversion and transmit the upper peak signals without clipping. A 4-pixel ImR with $1mm$ pixel side length is assumed to have optics with $5mm$ focal length, aperture of $1mm^2$ area and arranged in a 2×2 grid. A 4-element NImR is modeled to have 4 photodiodes of side length $1mm$, $1mm$ pitch, and a concentrator with 1.5 refractive index arranged in a 2×2 grid. The receivers are assumed located in the center, facing upwards, and at a distance of $2m$ from the transmitter plane. The transmitter side length is assumed

small enough that its image lies entirely inside the corresponding pixel of the ImR. Additionally, these MIMO systems are compared against an equivalent SISO system that receives the same amount of average optical flux as in the MIMO systems.

In an indoor VLC environment, the propagation delay of light rays from luminaires to receiver is of the order of a few nano-seconds where as the modulation bandwidth is of the order of few tens of mega-Hertz. Additionally, the multipath reflected signals undergo path-loss of the order of 100dB as compared to line-of-sight (LOS) signals. Thus only LOS signals are considered. In such scenario, $\mathbf{H}$ with the ImR is given by (3.6a), with NImR is given by (3.6b) and for the SISO system is 0.8979×10^{-7}. Note, in SIS-OFDM, since only 1 luminaire is active at a given time, the average transmitted flux per luminaire is assumed same as in the SISO system. Since all systems must receive the same amount of flux at same illumination levels, the point-to-point channel gains in each case are similar.

$$\mathbf{H} = 10^{-7} \times \begin{bmatrix} 0 & 0 & 0 & 0.8979 \\ 0 & 0 & 0.8979 & 0 \\ 0 & 0.8979 & 0 & 0 \\ 0.8979 & 0 & 0 & 0 \end{bmatrix} \tag{1.20a}$$

$$\mathbf{H} = 10^{-7} \times \begin{bmatrix} 0.8981 & 0.8979 & 0.8979 & 0.8977 \\ 0.8979 & 0.8981 & 0.8977 & 0.8979 \\ 0.8979 & 0.8977 & 0.8981 & 0.8979 \\ 0.8977 & 0.8979 & 0.8979 & 0.8981 \end{bmatrix} \tag{1.20b}$$

As mentioned before, for indoor VLC, transmitters must perform dual function of providing wireless data communication while maintaining appropriate average illumination level. Thus, to perform a fair comparison between SIS-OFDM systems implementing ACO-OFDM and DCO-OFDM, both techniques are compared at the same average emitted flux levels while maintaining almost equal bit-rates. This necessitates a different definition of SNR. For this work, SNR is defined as the ratio of the average transmitted electrical power to noise power and is similar as in (Fath and

Haas, 2013).

$$SNR_{avg}^{tx} = \frac{(hP_{avg}^{tx})^2}{N_0} \tag{1.21}$$

where P_{avg}^{tx} is the average radiant flux emitted by a transmitter, h is the optical to electrical conversion factor ($AW^{-1}\Omega^{-2}$) and N_0 is the noise power. Without loss of generality, $h = 1$ is assumed. Given the channel matrix in (3.6), the definition of SNR in (3.7) has an SNR offset of ≈ 150 dB over received signal power to noise power ratio. Using $N_{sc} = 64$, performance of ACO-OFDM with 16-QAM and 64-QAM is compared to that of DCO-OFDM with 4-QAM and 8-QAM respectively. This results in 192, 224, 190, and 221 bits per symbol respectively for the four configurations.

The effect of DC bias on system performance is studied using SNR vs DC offset curves to achieve a target BER= 10^{-3} and is illustrated in Figure3·2. The DC offset is set as a factor of the O-OFDM signal standard deviation (SD). In ACO-OFDM, all time-domain samples are clipped at zero thus increasing the probability of having active luminaires which don't emit any radiant flux. In this case, the receiver cannot identify the active luminaire, introducing significant errors in spatial-bit estimation. To deal with this issue, we apply a DC offset to ensure active luminaires emit a minimum radiant flux corresponding to the chosen offset. As the offset increases, the minimum flux received from the active transmitter progressively increases and thus improving error performance in determining the luminaire index. The optimal offset is empirically estimated to be 0.2×SD for ACO-OFDM with 64-QAM subcarrier modulation. Further increasing the offset value quickly gives diminishing returns in luminaire index detection. For DCO-OFDM, noise induced due to clipping of negative samples is not orthogonal to data subcarriers. Thus at small offsets, a large proportion of signal gets clipped causing significant bit errors. The simulations confirm that an offset of 3.2×SD is needed to sustain a link using DCO-OFDM.

Different SIS-OFDM systems are compared at their optimal DC offsets as empir-

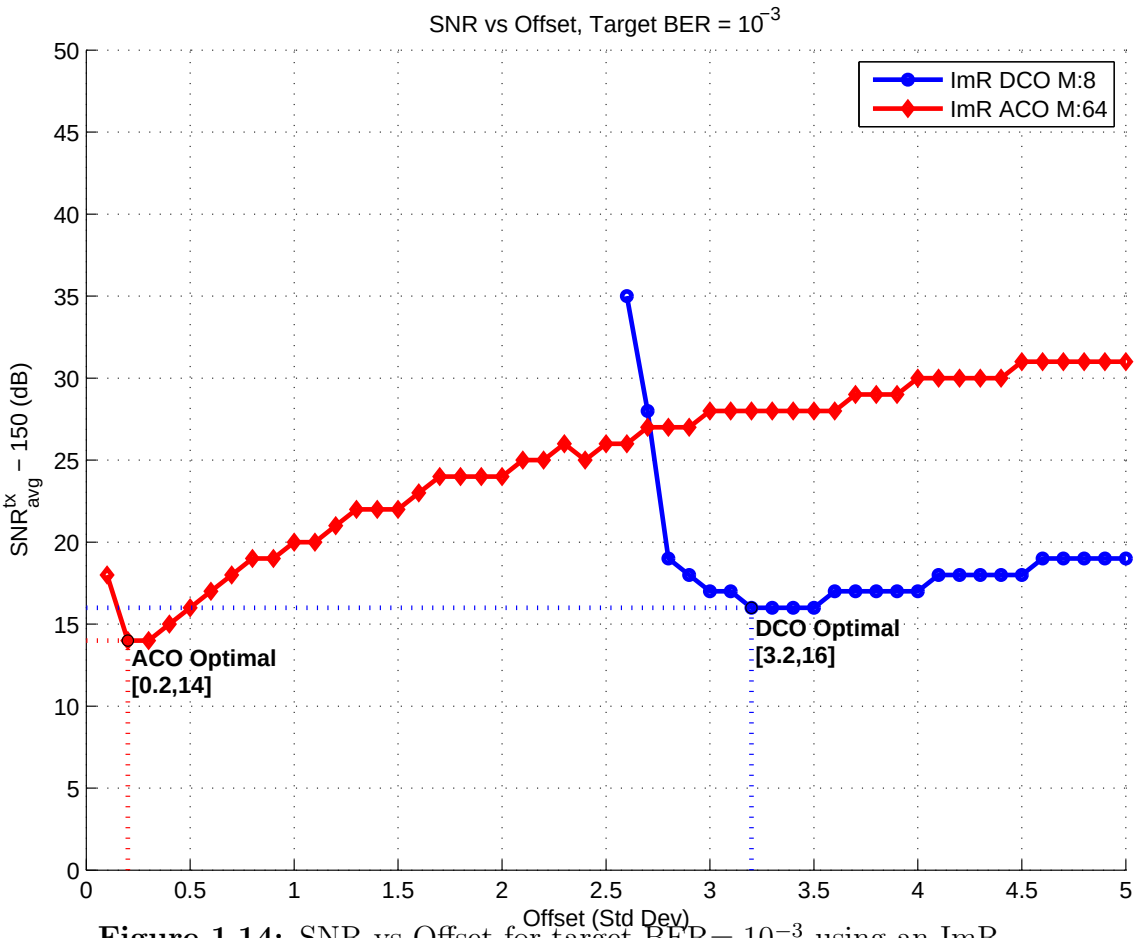

Figure 1·14: SNR vs Offset for target BER= 10^{-3} using an ImR

ically determined from Figure3·2. BER vs SNR curves at optimal DC offsets equal to 0.2×SD for ACO-OFDM with 64-QAM subcarrier modulation and 3.2×SD for DCO-OFDM with 8-QAM subcarrier modulation using ImR and NImR are illustrated in Figure3·3. It is shown that using ImR can provide significant SNR gain (≈135dB) over NImR for BER= 10^{-3}. For the NImR, each photodiode receives significant signal from each of the 4 luminaires and thus high ICI is expected. The ImR provides channel decorrelation thus significantly improving the system performance. As seen from the figure, it is impractical to achieve ≈150dB SNR for SIS-OFDM with NImR. The above SIS-OFDM configurations are compared with reference SISO O-OFDM systems. To achieve nearly the same bits/symbol as in the SIS-OFDM

systems, DCO-OFDM with 128-QAM subcarrier modulation and ACO-OFDM with 128^2-QAM subcarrier modulation yielding 217 and 224 bits/symbol are required. It is impractical to achieve ≈30dB SNR to achieve target BER performance at comparable spectral efficiencies for SISO O-OFDM systems with higher order subcarrier modulation. The SIS-OFDM system with ImR not only provides better spectral efficiency but also achieves the target BER at lower transmit powers. Additionally, the ImR considered has practical dimensions and can be incorporated in portable devices.

BER vs SNR curves for individual O-OFDM and OSM streams for the SIS-OFDM systems considered are shown in Figure3·4. At low SNR, bit errors are dominated by errors in luminaire index detection. Errors in luminaire index leads to choosing a different signal value for decoding the O-OFDM signal, thus introducing additional errors in O-OFDM signal decoding. As the SNR increases, errors in transmitter index detection significantly decrease and errors in O-OFDM symbol decoding dominates the BER. As the SNR is further increased, errors in the O-OFDM symbol decoding decrease thus reducing the overall BER.

In conclusion, we show that a system implementing SIS-OFDM can achieve additional $R^s = N_{sc} \times log_2(N_{tx})$ bits per symbol of spectral efficiency as compared to SISO O-OFDM systems. Results indicate that the use of an ImR provides additional channel decorrelation and can help achieve up to 130dB improvement in SNR when compared to system performance using a NImR. At significantly lower computational complexity, the SIS-OFDM can provide an additional $(3 \times N_{sc} \times k/4)$ bits per symbol for ACO-OFDM and $((N_{sc}/2-1) \times k)$ bits per symbol for DCO-OFDM over recently proposed approaches that combine OSM with O-OFDM.

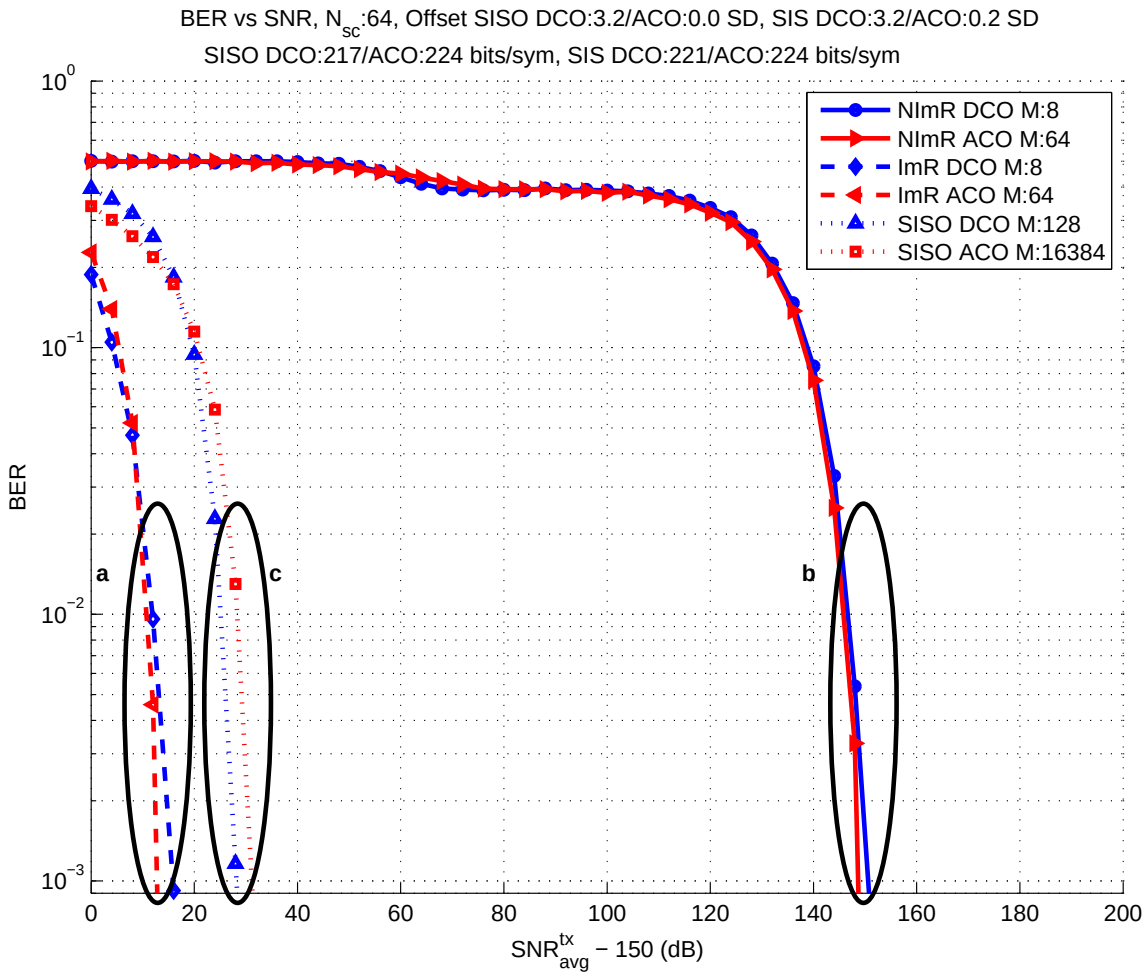

Figure 1·15: Comparison of BER vs SNR for (a) ImR, (b) NImR and (c) SISO

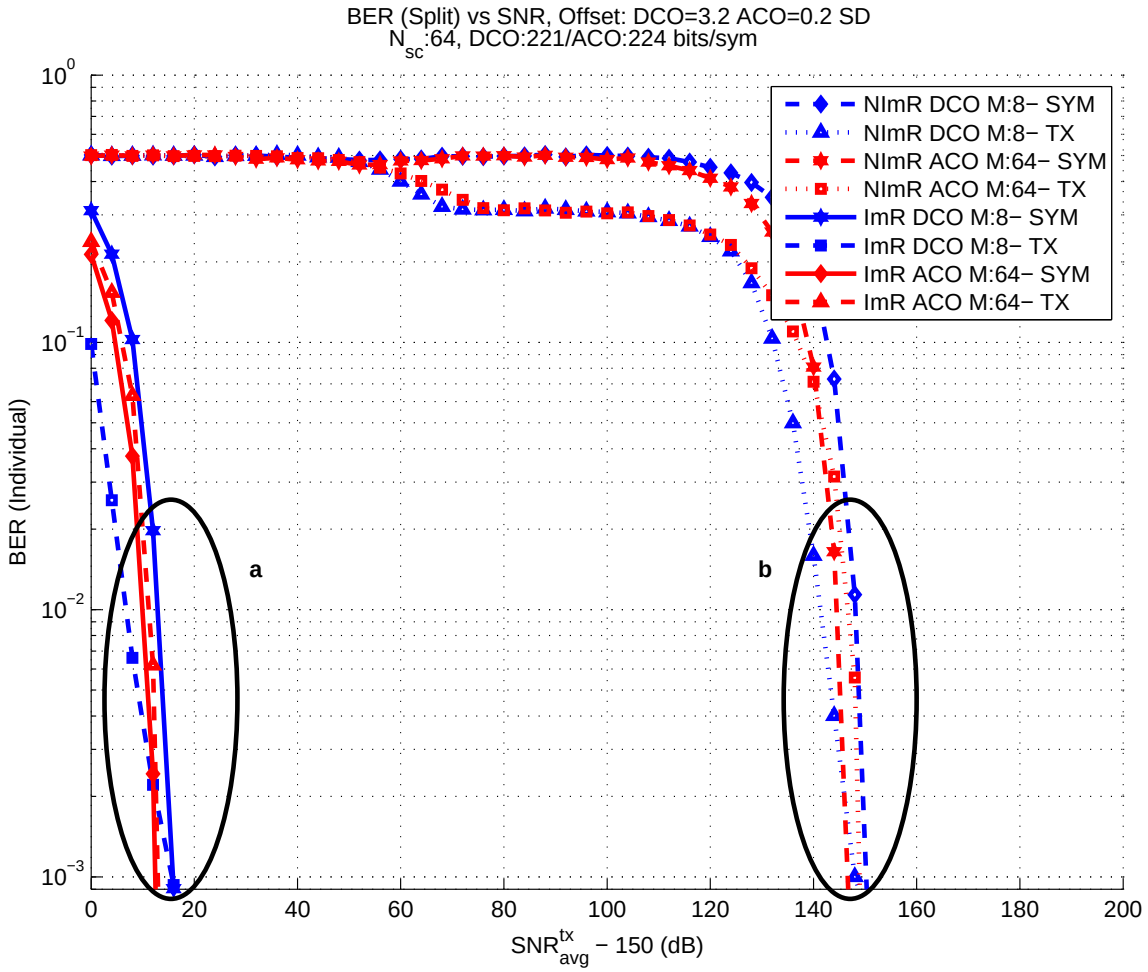

Figure 1·16: Comparison of individual BER vs SNR for (a) ImR and (b) NImR

References

Armstrong, J. and Lowery, A. (2006). Power efficient optical ofdm. *Electronics Letters*, 42(6):370 – 372.

Butala, P. M., Elgala, H., and Little, T. D. (2013). Svd-vlc: A novel capacity maximizing vlc mimo system architecture under illumination constraints. In *Globecom Workshops (GC Wkshps), 2013 IEEE*, pages 1087–1092.

Butala, P. M., Elgala, H., and Little, T. D. (2014). Performance of optical spatial modulation and spatial multiplexing with imaging receiver. In *IEEE WCNC'14 Track 1 (PHY and Fundamentals) (IEEE WCNC'14 Track 1 : PHY)*, Istanbul, Turkey.

Elgala, H., Mesleh, R., and Haas, H. (2011). Indoor optical wireless communication: potential and state-of-the-art. *Communications Magazine, IEEE*, 49(9):56–62.

Fath, T. and Haas, H. (2013). Performance comparison of mimo techniques for optical wireless communications in indoor environments. *Communications, IEEE Transactions on*, 61(2):733–742.

Fath, T., Haas, H., Di Renzo, M., and Mesleh, R. (2011). Spatial modulation applied to optical wireless communications in indoor los environments. In *Global Telecommunications Conference (GLOBECOM 2011), 2011 IEEE*, pages 1–5.

Ganesan, S., Mesleh, R., Haas, H., Ahn, C. W., and Yun, S. (2006). On the performance of spatial modulation ofdm. In *Signals, Systems and Computers, 2006. ACSSC '06. Fortieth Asilomar Conference on*, pages 1825–1829.

Mesleh, R., Elgala, H., and Haas, H. (2011). On the performance of different ofdm based optical wireless communication systems. *Optical Communications and Networking, IEEE/OSA Journal of*, 3(8):620 –628.

Mesleh, R., Mehmood, R., Elgala, H., and Haas, H. (2010). Indoor mimo optical wireless communication using spatial modulation. In *Communications (ICC), 2010 IEEE International Conference on*, pages 1 –5.

Popoola, W., Poves, E., and Haas, H. (2012). Spatial pulse position modulation for optical communications. *Lightwave Technology, Journal of*, 30(18):2948–2954.

Zhang, X., Dimitrov, S., Sinanovic, S., and Haas, H. (2012). Optimal power allocation in spatial modulation ofdm for visible light communications. In *Vehicular Technology Conference (VTC Spring), 2012 IEEE 75th*, pages 1–5.